Research Article

Mathematical Methods in the Applied Sciences

Received XXXX

(www.interscience.wiley.com) DOI: 10.1002/sim.0000
MOS subject classification: 35Q20, 35L03, 65M08, 65M12, 82D30

Asymptotic preserving numerical schemes for a non-classical radiation transport model for atmospheric clouds

Kai Krycki[a], Christophe Berthon[b], Martin Frank[a], Rodolphe Turpault[b]

We present numerical schemes for the P1- and M1-moment approximations of a non-classical transport equation modelling radiative transfer in atmospheric clouds. In contrast to classical radiative transfer, the photon path-length is introduced as an additional variable and serves as pseudo-time in this model. Since clouds may have optically thick regions, we introduce a diffusive scaling and show that the diffusion limits of the moment models and the original equations agree. Furthermore, we show that the numerical schemes also preserve the diffusion asymptotics as well as the set of admissible and realizable states, both for the explicit and the implicit discretization of the pseudo-time variable. A source iteration-like method is proposed and we observe that it converges slowly in the optical thick case, but a suitable initialisation can help to overcome this problem. We validate our method in 1D and present simulation results in the 2D-case for real cloud data.

Keywords: Non-classical transport; Radiative Transfer; Asymptotic Preserving Schemes

1. Introduction

The interaction of solar radiation and atmospheric clouds is one of the major challenges in global climate modelling because of its influence on the radiation budget of the earth. It is still one of the main sources of uncertainty in current climate model predictions. Classical radiative transfer models have shown wrong predictions in the past. Some researchers [1] suppose that the structure of the background medium has to be taken into account, so Larsen [2, 3] suggested the following non-classical transport equation to model the transfer of photons in atmospheric clouds:

$$\partial_s \phi(s,x,v) + v\nabla_x \phi(s,x,v) + \Sigma_t(s)\phi(s,x,v) = 0 \tag{1a}$$

$$\phi(0,x,v) = c\int_0^\infty \int \sigma(v,v')\Sigma_t(s')\phi(s',x,v')dv'ds' + Q(x,v), \tag{1b}$$

where $s \in (0,\infty)$, $x \in \mathbb{R}^N$, $v \in S^{N-1}$ the unit sphere in $\mathbb{R}^N$. Here, $\phi(s,x,v)$ is the angular particle flux at point x into direction v. The introduction of an additional variable s, which is the path length travelled by the particle since its previous interaction, makes this equation "non-classical". Note that the scattering frequency Σ_t depends explicitly on s. The path length s can also be seen as the time elapsed since the previous interaction and can hence be treated as a pseudo time variable. Therefore (1) has an interpretation as an initial value problem with respect to s, with the distinctive feature that the initial value is a functional of the full solution. It has been shown in [4] that a unique and non negative solution of (1) exists under reasonable assumptions.

To derive this model, the following simplifications have to be made. An atmospheric cloud is assumed to be an infinite and statistically homogeneous collection of water droplets of equal size which are randomly distributed in space. Furthermore, energy

[a] *RWTH Aachen University, Center for Computational Engineering Sciences, Schinkelstrasse 2, 52062 Aachen - Germany*
[b] *Université de Nantes, Laboratoire de Mathmatiques Jean Leray, 2, Rue de la Houssinire, 44322 Nantes Cedex 03 - France*
[*] *Correspondence to: Kai Krycki. E-mail: krycki@mathcces.rwth-aachen.de*

Contract/grant sponsor: This work was supported by RWTH Seed Funds Project 2010, funded by the Excellence Initiative of the German federal and state governments. The authors from Nantes were additionally supported by the MATPYL project - FR no. 2962.

or frequency of the photon is omitted. Then a photon interacts with the background medium by collisions with a scattering center, a water droplet in this case. The probability that a particle which has already travelled a distance s hits a water droplet is given by the scattering frequency $\Sigma_t(s)$. In case of a collision event, $0 < c < 1$ denotes the probability that the photon is scattered. Then, a photon with direction v changes its direction to v' due to a probability given by the scattering kernel $\sigma(v, v')$. With a probability of $1 - c$ the particle is absorbed. After scattering, the particle travels a certain distance until the next collision event occurs.
A probability density p for the distance between two collisions can be defined in terms of the scattering frequency Σ_t and vice versa:

$$p(s) = \Sigma_t(s) \exp\left(\int_0^\infty \Sigma_t(\tau) d\tau\right) \quad \text{or} \quad \Sigma_t(s) = \frac{p(s)}{1 - \int_0^s p(\tau) d\tau}. \tag{2}$$

Standard radiative transfer models assume that the positions of the scattering centres are uncorrelated and hence, the underlying distribution of scattering centres in space is Poisson-like. This results in an exponential decay of p due to the Beer-Lambert law. But this seems to disagree with current observations [5], which suggest that the path-length distribution decays algebraically and hence, non-exponential. It has been suggested [1] that this is rooted in a correlation of the locations of the scattering centres. One of the key features of this model is that it covers this case by the (possible) s-dependence of the scattering frequency. Since the s-value denotes the distance of a particle to its last scattering event, the variable s can also be interpreted as a memory variable.
Summing up, equation (1b) states that all photons which are scattered or injected into the system have zero distance to the last scattering event, while equation (1a) models the transport of the particles.
For $\Sigma_t \equiv \Sigma$ constant we have classical transport with an exponential attenuation law (see again [2]). In this case $p(s) = \Sigma \exp(-s\Sigma)$. To model a non-exponential attenuation law we will always use an algebraically decaying function of the form

$$\Sigma_t(s) = \frac{\alpha - 1}{s + 1} \quad \text{which means} \quad p(s) = \frac{\alpha - 1}{(s+1)^\alpha}, \quad \alpha > 3. \tag{3}$$

In this paper, we investigate numerical schemes to solve equation (1). As one can easily check by looking into the sky, an atmospheric cloud may have optically thick as well as optically thin regions. Therefore it is necessary to derive numerical schemes which are correct both in the optically thick, diffusive regime and in the transition regime. It is well known that numerical problems arise in the diffusive regime [6, 7] where length scales of different magnitudes come into play. A typical atmospheric cloud is several kilometres big, but the length of a typical photon free-path has a scale of metres. A numerical scheme can only yield reliable results if it covers the correct diffusion limit in the optically thick regime. Therefore we will first apply a diffusive scaling and derive an (analytical) diffusion approximation. Later on we will show that the limit of the numerical scheme in the diffusive limit is a discretization of this diffusion limit. If this is the case, the scheme will be called "asymptotic preserving". More on asymptotic preserving numerical schemes can be found in [8].

An additional difficulty for the solution of the full linear Boltzmann equation is that it is numerically costly due to its high dimensionality. In general, we have three space dimensions, two dimensions for the angle and an additional one dimensional path-length variable, which makes equation (1) a six-dimensional problem. A standard approach to reduce complexity of kinetic equations is the method of moments. The key idea is to derive a system of equations for its angular moments instead of solving the full equation. In this way, the kinetic variable is eliminated. These equations will then be called a moment model for equation (1). Since this system of equations will be under-determined one has to close the system by a moment closure, i.e. express the last moment in terms of the previous ones. The linear P1-closure, also referred to in the literature as the diffusion approximation, is based on a Legendre polynomial expansion of ϕ. In the context of radiative transfer, this closure has already been used in the early 40's [9]. The non-linear M1-closure is based on the minimum entropy principle, i.e. a functional of the moments is chosen which minimizes the radiative entropy and reproduces the lower order moments. The philosophical foundations for this approach were introduced in the 1950's in [10], while the first application in transport theory was made 20 years later in [11]. An application to the equation of radiative transfer can be found in [12]. When constructing a numerical scheme for a moment model, the numerical solution has to be both admissible and realizable [13]. Admissibility means that the scheme yields values in the area of definition of the moment closure (which is not defined everywhere in the M1 case). Realizability on the other hand means that the resulting approximations are in fact the first two moments of an angular distribution. It will turn out that both are conditions on the relative flux, which is the fraction of the first over the zeroth moment.

The remainder of this paper is organized as follows. We give a short overview on the diffusive scaling and the analytical diffusion limit in section 2. Due to the high dimensionality of the full equation moment models of reduced complexity are derived by introducing angular moments in section 3. Therein, we will investigate both the P1 and the M1 moment closure. In section 4, numerical schemes for the moment models are introduced and we show that they preserve the diffusion asymptotics. This is done both for the explicit and the implicit time-discretization. Furthermore, results on L^2-stability and the preservation of the set of admissible and realizable states are proven. Coupling of the initial value to the full solution strongly suggests to solve the system iteratively. Hence, in section 5 we introduce a source iteration-like method and perform a von Neumann stability analysis for this method. We observe that the iteration becomes arbitrarily slow in the optical thick case. Moreover, we present an initialization strategy for this iteration. Finally, numerical results for the 1D and 2D case are presented in section 6 and a short conclusion and outlook are given in the last section 7.

2. Scaling and the Diffusion Limit

An atmospheric cloud may have optically thick regions where transport of photons is dominated by scattering, therefore we apply the following scaling. It relies on the assumption that the probability for absorption is small and scattering is not forward-peaked, as it was introduced in [14]. A detailed analysis of the diffusion asymptotics can be found in [2, 3, 4]; we only give a sketch of it here.
For the rest of this paper we define the first and second moment of the path-length distribution as

$$\langle s\rangle := \int_0^\infty s p(s) ds, \quad \langle s^2\rangle := \int_0^\infty s^2 p(s) ds.$$

Now, let $0 < \varepsilon \ll 1$, then we scale the parameters Q, Σ_t and c as follows:

$$Q \to \varepsilon Q, \quad \Sigma_t(s) \to \frac{1}{\varepsilon}\Sigma_t(s/\varepsilon), \quad c \to 1 - \kappa\varepsilon^2,$$

where $\kappa > 0$. By additionally scaling the pseudo time-scale by

$$\phi_\varepsilon(s, x, v) := \phi(s\varepsilon, x, v),$$

the new scaled unknown satisfies

$$\partial_s \phi_\varepsilon(s, x, v) + \varepsilon v \nabla_x \phi_\varepsilon(s, x, v) + \Sigma_t(s)\phi_\varepsilon(s, x, v) = 0;$$
$$\phi_\varepsilon(0, x, v) = (1 - \kappa\varepsilon^2)\int_0^\infty \int \sigma(v, v')\Sigma_t(s')\phi_\varepsilon(s', x, v') dv' ds' + \varepsilon Q(x, v).$$

This equation can be further simplified. By setting

$$\Phi_\varepsilon = \varepsilon\langle s\rangle \exp\left(\int_0^s \Sigma_t(\tau) d\tau\right) \phi_\varepsilon(s, x, v)$$

we make use of (2), and the equation now reads

$$\partial_s \Phi_\varepsilon + \varepsilon v \nabla_x \Phi_\varepsilon = 0; \tag{4a}$$
$$\Phi_\varepsilon(0, x, v) = (1 - \kappa\varepsilon^2)\int_0^\infty \int \sigma(v, v') p(s) \Phi_\varepsilon(s', x, v') ds' dv' + \varepsilon^2\langle s\rangle Q(x, v). \tag{4b}$$

Applying a formal Hilbert expansion in the parameter ε by

$$\Phi_\varepsilon = \Phi_0 + \varepsilon\Phi_1 + \varepsilon^2\Phi_2 + \cdots$$

and letting $\varepsilon \to 0$, one derives the following diffusion approximation (see again [2, 3] or [4] for the details):

$$-\frac{1}{3}\left(\frac{\langle s^2\rangle}{2} + \frac{\bar\mu_0}{1 - \bar\mu_0}\right)\nabla_x^2\Phi_0 + \kappa\Phi_0 = \langle s\rangle Q(x), \tag{5}$$

with $\Phi_0 = \Phi_0(x)$ and $\bar\mu_0$ being the mean scattering cosine. In the following, we will always consider an isotropic medium with constant probability for the outgoing angle, and in this case we simply have $\bar\mu_0 = 0$. All combined, Φ_0 is an approximation of the classical angular radiation flux up to first order due to

$$\int_0^\infty \int \phi(s, x, v) dv ds = \Phi_0(x) + O(\varepsilon).$$

Note that this diffusion limit is not valid any more as soon as

$$p(s) \geq \frac{C}{s^3},$$

because in this case $\langle s^2\rangle = \infty$.

3. Moment Models

Solving the full linear Boltzmann equation is numerically costly due to its high dimensionality. Hence, we derive moment models for equation (1) in order to reduce complexity. Introducing the first three angular moments of function ϕ given by

$$E(s, x) := \int \phi(s, x, v) dv, \quad F(s, x) := \int v\phi(s, x, v) dv,$$
$$P(s, x) := \int (v \otimes v)\phi(s, x, v) dv,$$

and by multiplying equation (4) by v and integrating over v, we obtain the following coupled system of linear transport equations:

$$\partial_s E + \varepsilon \nabla_x F = 0, \qquad \partial_s F + \varepsilon \nabla_x P = 0;$$
$$E(0,x) = \varepsilon^2 \langle s \rangle Q(x) + (1 - \kappa\varepsilon^2) \int_0^\infty p(s) E(s,x) ds, \quad F(0,x) = 0.$$

Note that we have only two equations for three unknown functions. Therefore, we apply two different moment closures of the form $P = P(E,F)$ to this system of equations. We set $f := \|\frac{F}{E}\|$. The linear P1-model is based on a Legendre polynomial expansion of ϕ and gives

$$P = \chi(f) E = \frac{E}{3} \mathrm{Id},$$

where Id is the identity tensor and χ, the so-called Eddington factor, is constant in this case. The second moment closure we will use is the M1-model based on the minimum entropy principle. The M1 closure leads to a coupled system of non-linear partial differential equations with

$$P = \left(\frac{1-\chi(f)}{2} \mathrm{Id} + \frac{3\chi(f)-1}{2} \frac{F \otimes F}{\|F\|^2} \right) E,$$

where the Eddington factor in this case is given by

$$\chi(f) := \frac{3 + 4f^2}{5 + 2\sqrt{4 - 3f^2}}.$$

In the one dimensional case the closure relations reduce to $P = E/3$ for the P1-model and

$$P = \frac{3 + 4f^2}{5 + 2\sqrt{4 - 3f^2}} E$$

for the M1-model. Hence, the system becomes

$$\partial_s E + \varepsilon \nabla_x F = 0, \qquad \partial_s F + \varepsilon \nabla_x \chi(F/E) E = 0; \tag{6a}$$
$$E(0,x) = \varepsilon^2 \langle s \rangle Q(x) + (1 - \kappa\varepsilon^2) \int_0^\infty p(s) E(s,x) ds, \quad F(0,x) = 0, \tag{6b}$$

with χ being linear in the P1- and nonlinear in the M1-model.
Let us now show that both the $M1$ and $P1$ models have the relevant asymptotic limit when $\varepsilon \to 0$. To do so, we perform a Hilbert expansion of E and F:

$$E = E_0 + \varepsilon E_1 + \varepsilon^2 E_2 + \dots,$$
$$F = F_0 + \varepsilon F_1 + \varepsilon^2 F_2 + \dots$$

and we define

$$\Pi_i(x) = \int_0^\infty p(s) E_i(s,x) ds.$$

Inserting these expansions into the system (6) and identifying the powers of ε, we get :

$$\underline{\varepsilon^0 \text{ terms:}} \qquad E_0 = \Pi_0 = \int_0^\infty p(s) E_0(s,x) ds, \quad F_0 = 0.$$

Since $F_0 \equiv 0$, we note that F is of order ε and so is $f = \frac{F}{E}$ (assuming $E \neq 0$ everywhere). Then we have in the M1 case

$$\chi(f) = \frac{1}{3} + \frac{1}{2} f^2 + \frac{3}{32} f^4 + \mathrm{O}(f^6)$$

near $f = 0$. Consequently, both in the P1- and the M1-case,

$$\chi(F/E) E = \frac{1}{3} E + \mathrm{O}(\varepsilon). \tag{7}$$

Hence, we can continue by

$$\underline{\varepsilon^1 \text{ terms:}} \qquad E_1 = \Pi_1, \quad F_1 = -\frac{s}{3} \partial_x \Pi_0.$$

Inserting this into the next set of equations yields:

$$\underline{\varepsilon^2 \text{ terms:}} \qquad E_2 = \frac{s^2}{2} \frac{1}{3} \partial_x^2 \Pi_0,$$
$$-\frac{1}{3} \frac{\langle s^2 \rangle}{2} \partial_x^2 \Pi_0 + \kappa \Pi_0 = \langle s \rangle Q.$$

This last equation coincides with (5) if scattering is isotropic, i.e. when the mean scattering cosine $\mu_0 = 0$.

4. Asymptotic Preserving Numerical Schemes

In this section we investigate properties of numerical schemes for the moment models of (1) which have been derived in the previous section. Since the parameter ε is assumed to be small, we will especially investigate the behaviour of these schemes in the diffusive limit $\varepsilon \to 0$.
To simplify the notation we set $E(s,x) := E(s,x)$ and $F(s,x) := F(s,x)$. Furthermore, we choose a uniform time-space grid (s_n, x_i) with $s_{n+1} := s_n + \Delta s$ and $x_{i+1} := x_i + \Delta x$ for $n \in \mathbb{N}_0$ and $i \in \mathbb{Z}$. Then we use the abbreviations $Q_i := Q(x_i)$, $E_i^n := E(s_n, x_i)$ and $P_i^n := \chi(E_i^n, F_i^n)E_i^n$. Using HLL as a guideline (see [15]), one derives the following discretization scheme:

$$\frac{E_i^{n+1} - E_i^n}{\Delta s} + \varepsilon \frac{F_{i+1}^n - F_{i-1}^n}{2\Delta x} - \varepsilon^2 \frac{E_{i+1}^n - 2E_i^n + E_{i-1}^n}{2\Delta x} = 0, \tag{8a}$$

$$\frac{F_i^{n+1} - F_i^n}{\Delta s} + \varepsilon \frac{P_{i+1}^n - P_{i-1}^n}{2\Delta x} - \varepsilon^2 \frac{F_{i+1}^n - 2F_i^n + F_{i-1}^n}{2\Delta x} = 0, \tag{8b}$$

$$E_i^0 = (1 - \kappa\varepsilon^2) \sum_{n=0}^{\infty} \omega_n p_n E_i^n \Delta s + \varepsilon^2 \langle s \rangle Q_i, \qquad F_i^0 = 0, \tag{8c}$$

for some infinite quadrature rule given by the weights ω_n. In practice the integration is cut off at some $s_{\max}$. This can be justified by the fact that p is a fast decaying function, hence, the contribution to the integral will be small for $s > s_{\max}$. The second central differences term is the typical numerical diffusion. The maximal and minimal signal speeds of the system are $\pm\varepsilon$, that explains the factor ε^2 in front of the diffusion term.

4.1. Explicit Scheme

In order to simplify calculations, we write the scheme in the following as:

$$E_i^{n+1} = E_i^n - \varepsilon\mu(F_{i+1}^n - F_{i-1}^n) + \varepsilon^2\mu(E_{i+1}^n - 2E_i^n + E_{i-1}^n), \tag{9a}$$

$$F_i^{n+1} = F_i^n - \varepsilon\mu(P_{i+1}^n - P_{i-1}^n) + \varepsilon^2\mu(F_{i+1}^n - 2F_i^n + F_{i-1}^n), \tag{9b}$$

$$E_i^0 = (1 - \kappa\varepsilon^2) \sum_{n=0}^{\infty} \omega_n p_n E_i^n + \varepsilon^2 \langle s \rangle Q_i, \;\; F_i^0 = 0, \tag{9c}$$

where $\mu = \frac{\Delta s}{2\Delta x}$. The first problem we will address in this section is the behaviour of the numerical scheme in the diffusive limit. A numerical scheme is called asymptotic preserving, if for each fixed discretization the leading order of the numerical solution is governed by a discretization of the correct analytic diffusion limit as ε tends to 0. As in the previous section we will apply a Hilbert expansion argument. This is a systematic formal procedure to identify one solution in the ring of formal power series in ε with coefficients in a suitable function space. We will not give a rigorous proof for uniform convergence in ε here. When strong nonlinearities are concerned, more rigorous proofs are out of reach. Therefore most works use a similar formal ansatz [16, 17, 18]. Rigorous results exist only for linear [19] and quasi-linear kinetic equations [20].

Proposition 1. *Assume the quadrature satisfies the following relation:*

$$\sum_{n=0}^{\infty} \omega_n p_n = 1. \tag{10}$$

Then, the numerical scheme (9) is asymptotic-preserving i.e. it degenerates into a scheme consistent with (5) when $\varepsilon \to 0$. Furthermore, the limit scheme is second-order accurate if the following condition holds:

$$\sum_{n=0}^{\infty} n\omega_n p_n = 0. \tag{11}$$

Proof. Mimicking the continuous case, we perform a Hilbert expansion of E_i^n and F_i^n:

$$E_i^n = E_{0,i}^n + \varepsilon E_{1,i}^n + \varepsilon^2 E_{2,i}^n + \dots,$$
$$F_i^n = F_{0,i}^n + \varepsilon F_{1,i}^n + \varepsilon^2 F_{2,i}^n + \dots$$

We also define $\Pi_i := \sum_{n=0}^{\infty} \omega_n p_n E_{0,i}^n$. Now, plugging these expansions into the scheme (9) and identifying the powers of ε, we get:

- order (ε^0):

$$E_{0,i}^n = \Pi_i = \sum_{n=0}^{\infty} \omega_n p_n E_{0,i}^n,$$
$$F_{0,i}^n = 0.$$

  which is valid as soon as the quadrature weights ω_n satisfy the asumption (10).

- order (ε^1):
$$F_{1,i}^{n+1} = F_{1,i}^n - \frac{1}{3}\mu(\Pi_{i+1} - \Pi_{i-1}) = -(n+1)\frac{1}{3}\mu(\Pi_{i+1} - \Pi_{i-1}), \tag{12}$$
by summing up both sites from 0 to n.
- order (ε^2):
$$E_{2,i}^{n+1} = E_{2,i}^n - \mu(F_{1,i+1}^n - F_{1,i-1}^n) + \mu(\Pi_{i+1} - 2\Pi_i + \Pi_{i-1}),$$
$$E_{2,i}^0 = \sum_{n=0}^{\infty} \omega_n p_n E_{2,i}^n - \kappa\Pi_i + \langle s\rangle Q_i.$$
Inserting (12) inside the first equation and summing over n, then inserting this into the the second equation gives:
$$-\frac{1}{3}\sum_{n=0}^{\infty}\frac{n(n-1)}{2}\Delta s^2\omega_n p_n\frac{\Pi_{i+2} - 2\Pi_i + \Pi_{i-2}}{4\Delta x^2}$$
$$-\Delta x\sum_{n=0}^{\infty}\Delta s n\omega_n p_n\frac{\Pi_{i+1} - 2\Pi_i + \Pi_{i-1}}{\Delta x^2} + \kappa\Pi_i = \langle s\rangle Q_i,$$
which is consistent with (5). Furthermore, this is a second order approximation under the condition (11).

□

Remark. *Note that p is a probability density and the left-hand side of condition (11) is a discretization of the first moment of p. Consequently this requires that at least some of the weights ω_n are negative which is non-standard and usually not desirable.*

Remark. *As we have seen in the previous section (7), the zeroth order term of $P(E,F)$ is $\frac{1}{3}E$ both in the P1 and in the M1-case. Consequently, this calculation is independent from the closure and the theorem is true for the P1 and the M1 case.*

The M1 closure is a function of the relative flux F/E and is not defined everywhere. We immediately see that χ is only defined if $F/E \leq 4/3$. Hence, this is a necessary condition for admissibility. Furthermore, F and E have to be realizable as first and zeroth moment of an angular distribution. This is mathematically equivalent to the condition $||F/E|| < 1$, which is both for the M1 and the P1 case. Covering both conditions, the following theorem holds.

Theorem 1. *There is $\Delta s_0 > 0$ such that if $\Delta s < \Delta s_0$, the numerical scheme (9) preserves the convex set of admissible and realizable states $\Omega = \{(E,F) \mid E > 0, \ \left\|\frac{F}{E}\right\| < 1\}$.*

Proof. We define $U_i^n := (E_i^n, F_i^n)^\top$ and $G(U_i^n) := (\varepsilon F_i^n, \varepsilon P_i^n)^\top$ so that we can write the scheme (9) in the usual compact form:
$$U_i^{n+1} = U_i^n - \frac{\Delta s}{\Delta x}(\mathcal{F}_{i+1/2}^n - \mathcal{F}_{i-1/2}^n),$$
with numerical flux
$$\mathcal{F}_{i+1/2}^n = \mathcal{F}(U_i^n, U_{i+1}^n) = \frac{1}{2}(G(U_{i+1}) - G(U_i^n)) - \frac{\varepsilon^2}{2}(U_{i+1}^n - U_i^n).$$
The scheme may be interpreted as an approximate Riemann solver in the fashion of Harten, Lax and Van Leer (see section 3 in [15] for the abstract framework). It consists of two constant intermediate states separated by a stationary wave. Similar computations were carried out for the M1 model of classical radiative transfer in [18]. We will assume that the two other wave speeds are respectively $-b$ and b, where b is to be made precise later on. That means at each discrete point and in each discrete time step we consider a Riemann problem with left state U_L and right state U_R. Thus U has the following approximate form:
$$U(s,x) = \begin{cases} U_R & \text{if } \frac{x}{s} > b, \\ U_R^\star & \text{if } 0 < \frac{x}{s} < b, \\ U_L^\star & \text{if } -b < \frac{x}{s} < 0, \\ U_L & \text{if } \frac{x}{s} < -b, \end{cases}$$
where $U_L := (E_L, F_L)^\top$, $U_R := (E_R, F_R)^\top$, $U_L^\star := (E_L^\star, F_L^\star)^\top$ and $U_R^\star := (E_R^\star, F_R^\star)^\top$. This is also illustrated in Figure 1.

The approximate states $U_L^\star$ and $U_R^\star$ can be obtained as follows. The numerical flux of such an approximate Riemann solver can be expressed as a function of the intermediate states as in [15]:
$$\mathcal{F}(U_L, U_R) = G(U_R) - \frac{\Delta x}{2\Delta s}U_R + \frac{1}{\Delta s}\int_0^{\frac{\Delta x}{2}} U(s,x)dx.$$

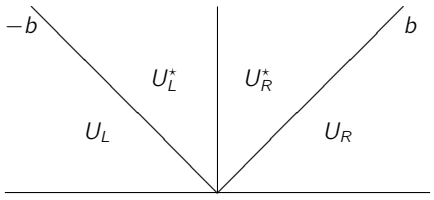

Figure 1. Illustration of the two-states approximate Riemann solver.

Using the form of the approximated solution $U(s,x)$, we have:

$$\mathcal{F}(U_L,U_R) = G(U_R) - \frac{\Delta x}{2\Delta s}U_R + b(U_R^\star - U_R)$$

which leads to:

$$\begin{aligned} U_R^\star &= U_R + \frac{1}{b}(\mathcal{F}(U_L,U_R) - G(U_R)) \\ &= U_R + \frac{1}{2b}\Big(G(U_L) - G(U_R) + \varepsilon^2(U_L - U_R)\Big). \end{aligned} \tag{13}$$

A similar computation yields:

$$U_L^\star = U_L + \frac{1}{2b}\Big(G(U_R) - G(U_L) + \varepsilon^2(U_L - U_R)\Big).$$

We first consider the values of b which ensure the positivity of $E_L^\star$ and $E_R^\star$:

$$\begin{aligned} E_R^\star &= E_R + \frac{\varepsilon}{2b}(F_L - F_R) + \frac{\varepsilon^2}{2b}(E_L - E_R), \\ E_L^\star &= E_L + \frac{\varepsilon}{2b}(F_R - F_L) + \frac{\varepsilon^2}{2b}(E_L - E_R), \end{aligned}$$

therefore $E_L^\star > 0$ and $E_R^\star > 0$ if:

$$b > b_1 := \frac{\varepsilon}{2}\max\Big(\frac{(F_R - F_L) + \varepsilon(E_R - E_L)}{E_R}, \frac{(F_L - F_R) + \varepsilon(E_R - E_L)}{E_L}\Big).$$

Then we consider the values of b which ensure the flux limitation i.e. $|F_L^\star| < E_L^\star$ and $|F_R^\star| < E_R^\star$:

$$F_R^\star = F_R + \frac{\varepsilon}{2b}(P_L - P_R) + \frac{\varepsilon^2}{2b}(F_L - F_R),$$

then $F_R^\star < E_R^\star$ and $-F_R^\star < E_R^\star$ if:

$$b > b_2 := \frac{\varepsilon}{2}\max\Big(\beta_{2,1}, \beta_{2,2}\Big)$$

where we have defined:

$$\begin{aligned} \beta_{2,1} &= \frac{P_L - P_R - F_L + F_R + \varepsilon(F_L - E_L - F_R + E_R)}{E_R - F_R}, \\ \beta_{2,2} &= \frac{-P_L + P_R - F_L + F_R + \varepsilon(-F_L - E_L + F_R + E_R)}{E_R + F_R}, \end{aligned}$$

and $P_L := P(E_L, F_L)$, $P_R := P(E_R, F_R)$. Similarly:

$$F_L^\star = F_L + \frac{\varepsilon}{2b}(P_R - P_L) + \frac{\varepsilon^2}{2b}(F_L - F_R),$$

then $F_L^\star < E_L^\star$ and $-F_L^\star < E_L^\star$ if:

$$b > b_3 := \frac{\varepsilon}{2}\max\Big(\beta_{3,1}, \beta_{3,2}\Big)$$

where:

$$\beta_{3,1} = \frac{P_R - P_L - F_L + F_R + \varepsilon(F_L - E_L - F_R + E_R)}{E_R - F_R},$$
$$\beta_{3,2} = \frac{-P_R + P_L - F_L + F_R + \varepsilon(-F_L - E_L + F_R + E_R)}{E_R + F_R}.$$

Finally, the CFL condition is given by the constraint of non-interacting waves:

$$\Delta s \leq \frac{\Delta x}{2b}.$$

Putting together the three former requirements on b, we obtain:

$$\Delta s \leq \Delta s_0 := \frac{\Delta x}{2\max(b_1, b_2, b_3)}. \tag{14}$$

□

Remark. *When $\varepsilon \to 0$, b_1, b_2 and b_3 defined in the former proof tend to zero, therefore $\Delta s_0 \to \infty$. As a consequence, the condition $\Delta s \leq \Delta s_0$ is not restrictive when asymptotic regimes are considered.*

Finally, using the Fourier transform, we can show the the explicit scheme is L^2-stable under a mild CFL condition in the linear P1 case. This is stated by the following lemma.

Lemma 1. *In the linear (P1) case i.e. when $P = \frac{1}{3}E$, the scheme (9) is L^2-stable under the CFL condition:*

$$\Delta s \leq \frac{2\Delta x}{\varepsilon^2 + \frac{1}{3} + \left|\frac{1}{3} - \varepsilon^2\right|}. \tag{15}$$

Proof. We introduce the auxiliary variables $U := F + E/\sqrt{3}$ and $V := F - E/\sqrt{3}$ to rewrite (9a)-(9b) as follows:

$$U_i^{n+1} = (1 - 2\varepsilon^2\mu)U_i^n - \frac{\varepsilon\mu}{\sqrt{3}}(U_{i+1}^n - U_{i-1}^n) + \varepsilon^2\mu(U_{i+1}^n - U_{i-1}^n),$$
$$V_i^{n+1} = (1 - 2\varepsilon^2\mu)V_i^n + \frac{\varepsilon\mu}{\sqrt{3}}(V_{i+1}^n - V_{i-1}^n) + \varepsilon^2\mu(V_{i+1}^n - V_{i-1}^n).$$

Now, we perform a discrete Fourier transform in space ($\hat{U}$ and $\hat{V}$ respectively represent the discrete Fourier transforms of U and V):

$$\hat{U}^{n+1} = A(\xi)\hat{U}^n, \quad \hat{V}^{n+1} = \overline{A(\xi)}\hat{V}^n,$$

with:

$$A(\xi) = (1 - 2\varepsilon^2\mu + 2\varepsilon^2\mu\cos(\Delta x\xi)) - \frac{2i\varepsilon\mu}{\sqrt{3}}\sin(\Delta x\xi)).$$

Therefore, the scheme is L^2-stable if and only if for all $\xi \in \mathrm{R}$ we have $|A(\xi)| \leq 1$. Since:

$$|A(\xi)|^2 - 1 = 4\varepsilon^2\mu(1 - \cos(\Delta x\xi))\Big(\varepsilon^2\big(1 - \cos(\Delta x\xi)\big) - 1 + \frac{1}{3}\mu\big(1 + \cos(\Delta x\xi)\big)\Big),$$

the scheme is stable if and only if the last term is positive for any $\xi \in \mathrm{R}$. Hence it is stable provided the following CFL condition holds:

$$\mu \leq \frac{1}{\varepsilon^2 + \frac{1}{3} + \left|\frac{1}{3} - \varepsilon^2\right|},$$

which is equivalent to (15). □

Even though the restrictions on Δs imposed by the former theorems are not extreme, our problem requires to iterate the computation of the approximate solutions up to the limit $s \to \infty$. Hence, it is more convenient to use an implicit scheme, especially for 2D and 3D simulations.

4.2. Implicit Scheme

We now consider the implicit version of the scheme (8):

$$E_i^{n+1} = E_i^n - \varepsilon\mu(F_{i+1}^{n+1} - F_{i-1}^{n+1}) + \varepsilon^2\mu(E_{i+1}^{n+1} - 2E_i^{n+1} + E_{i-1}^{n+1}), \tag{16a}$$

$$F_i^{n+1} = F_i^n - \varepsilon\mu(P_{i+1}^{n+1} - P_{i-1}^{n+1}) + \varepsilon^2\mu(F_{i+1}^{n+1} - 2F_i^{n+1} + F_{i-1}^{n+1}), \tag{16b}$$

$$E_i^0 = (1-\kappa\varepsilon^2)\sum_{n=0}^{\infty}\omega_n p_n E_i^n + \varepsilon^2\langle s\rangle Q_i,\ F_i^0 = 0, \tag{16c}$$

where $\mu = \frac{\Delta s}{2\Delta x}$ and $P_i^n = \chi(E_i^n, F_i^n)E_i^n$.

Proposition 2. *Assume the quadrature satisfies the condition (10), then the numerical scheme (16) is asymptotic-preserving i.e. it degenerates into a scheme consistent with (5) when $\varepsilon \to 0$.*
Furthermore, the limit scheme is second-order accurate if the condition (11) holds.

Proof. The proof is very similar to the explicit case. We perform an expansion of E_i^n and F_i^n:

$$E_i^n = E_{0,i}^n + \varepsilon E_{1,i}^n + \varepsilon^2 E_{2,i}^n + \dots,$$
$$F_i^n = F_{0,i}^n + \varepsilon F_{1,i}^n + \varepsilon^2 F_{2,i}^n + \dots$$

We also define $\Pi_i := \sum_n \omega_n p_n E_{0,i}^n$. Now, plugging these expansions into the scheme (16) and identifying the powers of ε, we get:

- order (ε^0):

$$E_{0,i}^n = \Pi_i = \sum_{n=0}^{\infty}\omega_n p_n E_{0,i}^n,$$
$$F_{0,i}^n = 0.$$

  which is valid as soon as the quadrature weights ω_n satisfy the assumption (10).
- order (ε^1):

$$F_{1,i}^{n+1} = F_{1,i}^n - \frac{1}{3}\mu(\Pi_{i+1} - \Pi_{i-1}) = -(n+1)\frac{1}{3}\mu(\Pi_{i+1} - \Pi_{i-1}), \tag{17}$$

  again by summation up to n.
- order (ε^2):

$$E_{2,i}^{n+1} = E_{2,i}^n - \mu(F_{1,i+1}^{n+1} - F_{1,i-1}^{n+1}) + \mu(\Pi_{i+1} - 2\Pi_i + \Pi_{i-1}),$$
$$E_{2,i}^0 = \sum_{n=0}^{\infty}\omega_n p_n E_{2,i}^n - \kappa\Pi_i + \langle s\rangle Q_i.$$

  Inserting (17) inside the first equation and summing over n, then inserting into the second equation gives:

$$-\frac{1}{3}\sum_{n=0}^{\infty}\frac{n(n+1)}{2}\Delta s^2\omega_n p_n\frac{\Pi_{i+2} - 2\Pi_i + \Pi i - 2}{4\Delta x^2}$$
$$-\Delta x\sum_{n=0}^{\infty} n\omega_n p_n\Delta s\frac{\Pi_{i+1} - 2\Pi_i + \Pi_{i-1}}{\Delta x^2} + \kappa\Pi_i = \langle s\rangle Q_i,$$

  which is consistent with (5). Furthermore, this is once again a second order approximation under the condition (11).

□

Remark. *Comparing the diffusion limit of the implicit and explicit scheme we observe the following. The dicretization of the diffusion coefficient $\langle s^2\rangle/2$ is given by*

$$\sum_{n=0}^{\infty}\frac{n(n+1)}{2}\Delta s^2\omega_n p_n \quad \textit{and} \quad \sum_{n=0}^{\infty}\frac{n(n-1)}{2}\Delta s^2\omega_n p_n$$

respectively. Both discretizations yield an error of order ds, which can be eliminated using a Crank-Nicholson scheme because of the alternating sign. The additional error term of order dx is not eliminated in this way.

5. Source Iteration

Solving the full system (8) directly is very costly because the initial value with respect to s is a functional of the solution itself. Therefore we apply an iterative method which is closely related to the classical source iteration method [7].
The idea of source iteration works as follows: choose initial data $E^{(0)}(s,x)$, and in every step solve

$$\partial_s E^{(n+1)} + \varepsilon \nabla_x F^{(n+1)} = 0, \qquad \partial_s F^{(n+1)} + \varepsilon \nabla_x \chi(F^{(n+1)}/E^{(n+1)}) E^{(n+1)} = 0; \tag{18a}$$

$$E^{(n+1)}(0,x) = (1-\kappa\varepsilon^2)\int_0^\infty p(s)E^{(n)}(s,x)ds + \varepsilon^2\langle s\rangle Q(x); \tag{18b}$$

$$F^{(n+1)}(0,x) = 0. \tag{18c}$$

This method is very simple simple and close to the physical interpretation. Thinking of the original equation (1), each iterate can be interpreted as the particles which have been scattered at most n times. A disadvantage of this method is that it converges very slowly (spectral radius ≈ 1), as we will show in the following.

5.1. Von Neumann Stability Analysis

We restrict our observation on the linear P1 case, but the results remain true if we use the M1 closure. The error between the iterate and the exact solution is

$$f^{(n+1)} := \begin{pmatrix} E - E^{(n+1)} \\ F - F^{(n+1)} \end{pmatrix} = \begin{pmatrix} \tilde{E}^{(n+1)} \\ \tilde{F}^{(n+1)} \end{pmatrix},$$

and it satisfies the equation

$$\partial_s \tilde{E}^{(n+1)} + \varepsilon \nabla_x \tilde{F}^{(n+1)} = 0, \qquad \partial_s \tilde{F}^{(n+1)} + \frac{\varepsilon}{3}\nabla_x \tilde{E}^{(n+1)} = 0; \tag{19a}$$

$$\tilde{E}^{(n+1)}(0,x) = (1-\kappa\varepsilon^2)\int_0^\infty p(s)\tilde{E}^{(n)}(s,x)ds, \tag{19b}$$

$$\tilde{F}^{(n+1)}(0,x) = 0. \tag{19c}$$

which is simply equation (18) without external source term. We now want to calculate the rate of convergence using a Fourier ansatz. Following [7], we define the quantity $\phi^{(n)}(x)$ as

$$\phi^{(n)}(x) := \int_0^\infty p(s)\tilde{E}^{(n)}(x,s)ds,$$

and apply the following Fourier ansatz. Here, $\omega(\lambda)$ is the contraction rate of the source iteration and the modes with respect to λ are defined as:

$$\phi^{(n)}(x) = \omega^n(\lambda)e^{i\lambda x}, \qquad \tilde{E}^{(n+1)}(s,x) = \omega^l(\lambda)\alpha(\lambda,s)e^{i\lambda x},$$
$$\phi^{(n+1)}(x) = \omega^l(\lambda)\gamma(\lambda)e^{i\lambda x}, \qquad \tilde{F}^{(n+1)}(s,x) = \omega^l(\lambda)\beta(\lambda,s)e^{i\lambda x}.$$

Inserting this into equations (19) and cancelling all common terms we get

$$\partial_s\alpha(\lambda,s) + i\lambda\varepsilon\beta(\lambda,s) = 0, \qquad \partial_s\beta(\lambda,s) + i\lambda\frac{\varepsilon}{3}\alpha(\lambda,s) = 0,$$
$$\alpha(\lambda,0) = (1-\kappa\varepsilon^2), \qquad \beta(\lambda,0) = 0.$$

We now insert the left into the right equation and multiply by $i\lambda\varepsilon$, which gives us

$$-\partial_s^2\alpha(\lambda,s) - \frac{\lambda^2\varepsilon^2}{3}\alpha(\lambda,s) = 0,$$

with initial conditions (with respect to s):

$$\alpha(\lambda,0) = 1-\kappa\varepsilon^2, \qquad \partial_s\alpha(\lambda,0) = -i\lambda\varepsilon\beta(\lambda,0) = 0.$$

The solution of this ordinary differential equation is given by

$$\alpha(\lambda,s) = (1-\kappa\varepsilon^2)\cos(\frac{1}{\sqrt{3}}\lambda\varepsilon s).$$

So in a next step, we insert this into the definition of $\phi^{(n+1)}$ and also insert the Fourier ansatz to get

$$\gamma(\lambda) = \int_0^\infty p(s)\alpha(\lambda, s)ds.$$

If $\Sigma_t(s) \equiv \Sigma$, then we have $p(s) = \Sigma \exp(-s\Sigma)$ and we can calculate $\gamma(\lambda)$ as

$$\gamma(\lambda) = \int_0^\infty \Sigma \exp(-s\Sigma)(1-\kappa\varepsilon^2)\cos(\frac{1}{\sqrt{3}}\lambda\varepsilon s)\mathrm{ds} = (1-\kappa\varepsilon^2)\underbrace{\frac{\Sigma^2}{\Sigma^2 + \frac{1}{3}(\lambda\varepsilon)^2}}_{=:\Gamma_1}.$$

and we see that $\Gamma_1(\lambda) \approx 1$ for small $\lambda \cdot \varepsilon$, and it tends to 0 if λ becomes large. Hence, large modes are sufficiently suppressed while the small modes are responsible for slow convergence, which agrees with the results in [7]. If the function $p(s)$ decays algebraically as

$$p(s) = \frac{\alpha - 1}{(s+1)^\alpha}, \quad \alpha > 3,$$

we have

$$\gamma(\lambda) = (1-\kappa\varepsilon^2)\underbrace{\int_0^\infty \frac{(\alpha-1)}{(s+1)^\alpha}\cos(\frac{1}{\sqrt{3}}\lambda\varepsilon s)\mathrm{ds}}_{=:\Gamma_2}.$$

This integral does not have a closed representation, numerical experiments using Maple 13 ® also yield that

$$\Gamma_2(\lambda, \varepsilon) \approx 1, \ \Gamma_2(\lambda, \varepsilon) \leq 1,$$

for small values of ε, λ, where we chose $\alpha = 5$.

$\alpha = 5$	$\lambda = 100$	$\lambda = 1$	$\lambda = 0.1$
$\varepsilon = 1$	0.005	0.955435	0.999449
$\varepsilon = 0.1$	0.3103921	0.999449	0.9999944
$\varepsilon = 0.01$	0.955435	0.9999944	0.999999994

We see here that again the large modes are sufficiently suppressed while the small ones are not. Hence, we are in the same situation as in the case above. Consequently, for source iteration, the contraction rate is $\omega(\lambda) = \gamma(\lambda) \approx 1$ if ε is small.

5.2. *Initialisation*

The source iteration algorithm (18) requires a suitable initialisation to overcome the problem of slow convergence. One way to choose it is to remark that in the case of a $P1$ closure, the exact solution can be expressed in a simpler framework. Indeed, if we assume that (E, F) is the solution of the $P1$ problem, then:

$$\Pi(x) = \int_0^\infty p(s)E(s, x)ds,$$

and we calculate formally:

$$\begin{aligned}\Pi'(x) &= \int_0^\infty p(s)\partial_x E(s,x)ds = -\frac{3}{\varepsilon}\int_0^\infty p(s)\partial_s F(s,x)ds \\ &= -\frac{3}{\varepsilon}\Big[\partial_s p(0)E(0,x)\Big]_0^\infty + \frac{3}{\varepsilon}\int_0^\infty \partial_s p(s)F(s,x)ds \\ &= \frac{3}{\varepsilon}\int_0^\infty \partial_s p(s)F(s,x)ds.\end{aligned}$$

Now the second derivative of Π can be computed as

$$\begin{aligned}\Pi''(x) &= \frac{3}{\varepsilon}\int_0^\infty \partial_s p(s)\partial_x F(s,x)ds = -\frac{3}{\varepsilon^2}\int_0^\infty \partial_s p(s)\partial_s E(s,x)ds \\ &= -3\partial_s p(0)\langle s\rangle Q(x) + 3\kappa\partial_s p(0)\Pi(x) \\ &\qquad + \left(-\frac{3}{\varepsilon^2}\partial_s p(0)\Pi(x) + \frac{3}{\varepsilon^2}\int_0^\infty \partial_s^2 p(s)E(s,x)ds\right),\end{aligned}$$

# grid points	L^1	L^2	L^∞
128	2.30e-3	2.70e-2	6.66e-2
256	4.37e-4	1.20e-2	2.49e-2
512	5.41e-5	5.89e-3	8.99e-3
1024	1.97e-5	2.95e-3	4.94e-3
2048	4.43e-6	1.47e-3	3.33e-3

Table 1. 1D test-case: convergence table for $\varepsilon = 10^{-2}$.

and, if $\Sigma_t(s) \equiv \Sigma$ is constant, the last term becomes 0 and this equation reads

$$\Pi''(x) = 3\kappa\Sigma^2\Pi(x) - 3\Sigma^2\langle s\rangle Q(x). \tag{20}$$

Since in this case $\langle s\rangle = 1/\Sigma$ and $\langle s^2\rangle = 2/\Sigma^2$, equation (20) equals the diffusion approximation (5) for $\mu_0 = 0$. The solution of this ODE will be used as an initial guess in the algorithm (18), equipped with the boundary conditions of the system, even though it is not valid anymore when the $M1$ model is selected.
For nonconstant Σ_t the last term does not disappear, but we can neglect it and take the numerical solution of

$$\Pi''(x) = -3\kappa\partial_s p(0)\Pi(x) + 3\partial_s p(0)\langle s\rangle Q(x)$$

as an initial value for $\int_0^\infty p(s)E(s,x)ds$ in the iteration of (18).

6. Numerical Results

In this final section we present some numerical results for test cases in one and two space dimensions. In 1D we can explicitly calculate the exact solution for the P1-model and compare it to our solution. Furthermore, we examine the impact of different path-length distribution functions on the solution. In 2D, we investigate two test cases from the NASA database I3RC [21]. The first is an academic example called the 'step-cloud', another is the MMCR cloud where measurements of the optical densities for a real-world atmospheric cloud are given.

6.1. 1D Test Cases

6.1.1. Comparison with exact solution We first consider the $P1$ model with $p(s) = e^{-s}$. In this case, we recall that Π is the solution of the ODE (20), which is used as an initial guess in the algorithm (18). To do so, we use the classic finite differences scheme:

$$-\frac{\Pi_{i+1} - 2\Pi_i + \Pi_{i-1}}{\Delta x^2} + 3\kappa\Pi_i = 3Q(x_i).$$

Let us fix Q as follows:

$$Q(x) = \frac{4\pi^2 + 27\kappa}{27}\sin\Big(\frac{2\pi x}{3}\Big),$$

so that the exact solution satisfies:

$$E(s,x) = \frac{1}{2}\Big(1 + \frac{4\pi^2\varepsilon^2}{27}\Big)\Big[\sin\Big(\frac{2\pi}{3}(x - \frac{\varepsilon s}{\sqrt{3}})\Big) + \sin\Big(\frac{2\pi}{3}(x + \frac{\varepsilon s}{\sqrt{3}})\Big)\Big].$$

We clearly see on figure 2 that the adopted iterative method is in a very good agreement with the exact solution. Furthermore, table 1 shows the error between the exact and approximated solutions in L^1, L^2 and L^∞ norm. The scheme is clearly order 1 in L^2 norm when ε is small.

6.1.2. Effect of the choice of p Here, we compare the effects of different choices of p on the solution. More precisely, we will consider:

$$p(s) = \exp(-s) \quad \text{or} \quad p(s) = \frac{\alpha - 1}{(s+1)^\alpha},$$

where $\alpha > 3$ in order that $\langle s\rangle$ and $\langle s^2\rangle$ are well defined. We choose $\varepsilon = 0.01$, $\kappa = 0.9$ and

$$Q(x) = \begin{cases} 1, & \text{if } -1 < x < 1, \\ 0, & \text{elsewhere.} \end{cases}$$

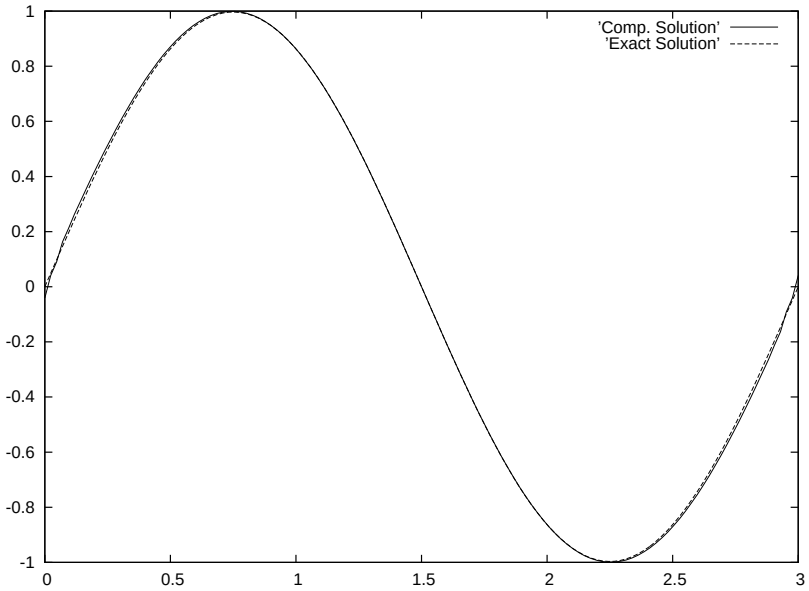

Figure 2. Comparison with exact solution at $s = 7$ with $\varepsilon = 10^{-2}$.

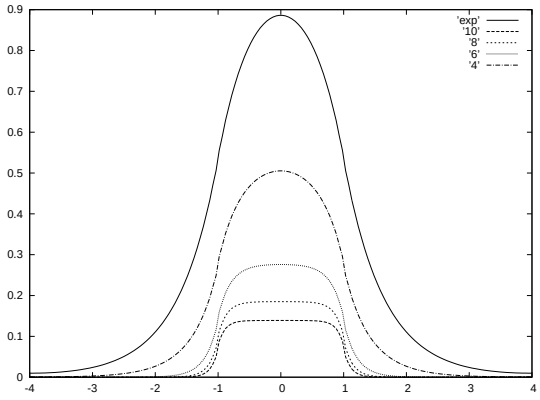

Figure 3. Values of Π for different choices of p. Full line: $p(s) = e^{-s}$.

This source term can be interpreted as a beam of photons which is inserted into the system at the central region. The computations where carried on a grid with $\Delta x = 32.10^{-3}$ m and the result is shown on figure 3. Note that these choices of p lead to different values of $\langle s \rangle$, which explains the differences on the maxima. For an increasing value of α the first moment of p decreases, hence the mean free-path is shorter and radiation intensity decreases.

6.2. 2D Test-Cases

In this section we consider two test cases taken from the NASA database I3RC. A detailed description of the test cases can be found in [21] (or here: http://i3rc.gsfc.nasa.gov). In both test cases the optical depth field is given which varies in space. That means, the assumption of a homogeneous medium does not hold here. Therefore, given the optical depth $\sigma(x)$, we consider a space dependent path-length distribution

$$p(s, x) = \sigma(x) \exp(-s\sigma(x)).$$

Note that this is only an approximation to the physically correct path length distribution at point x. We assume here that Σ_t is independent of s, and for each single x we choose $\Sigma_t = \sigma(x)$ constant.

Since all the simulations involve cartesian grids, they are performed using a simple directional splitting based on the 1D implicit scheme (16a)-(16b)-(16c), except for the last case where the explicit version (9a)-(9b)-(9c) is used. The source iteration algorithm is stopped when $\left\|\Pi^{n+1} - \Pi^n\right\| < 10^{-12}$.

6.2.1. Step Cloud The first simulations are based on the so-called "Step-Cloud Case". It consists of an academic juxtaposition of 250×250 m blocks. Each bloc is considered to have a constant optical depth, either 2 or 18 alternatively. As a result, we set $\Sigma_t(x) = \frac{2}{250} = 8.10^{-3}\ m^{-1}$ in the first regions and $\frac{18}{250} = 72.10^{-3}\ m^{-1}$ in the other regions.
We consider seven blocs with periodic boundary conditions and choose a 1750×25 mesh. The simulations are performed with source term $Q(x) = 1$ if $y < 50$ m and 0 elsewhere. First, we consider a case where $\varepsilon = 0.01$ and $\kappa = 0.85$. The settings imply

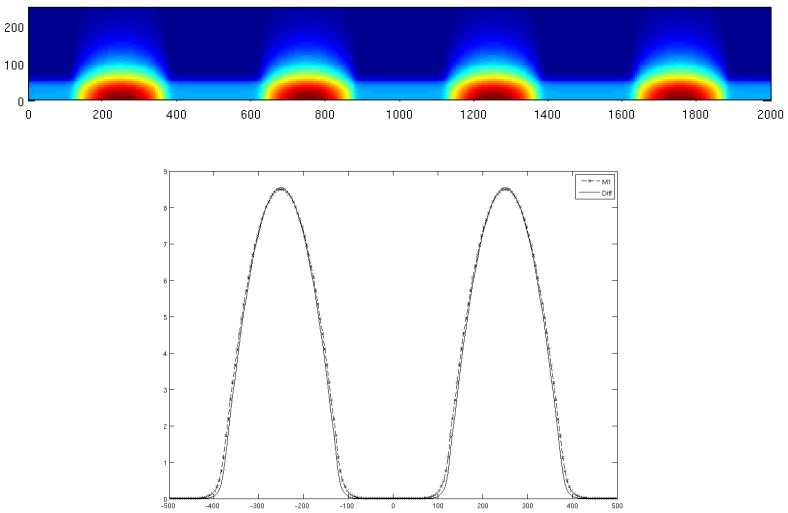

Figure 4. $\varepsilon = 0.01$, $F^0 = 0$.

that this is a pseudo-1D case. As expected, we see on figure 4 that the 1D and 2D codes provide very similar results here.
Now, in figure 5, we present the result obtained with different zenith angles. These angles are simulated by considering the following initial data for the radiative flux: $F_i^0 = (\cos(\theta), \sin(\theta))^\top E_i^0$. The other parameters are $\kappa = 0.85$ and $\varepsilon = 0.03$. We observe that the distinct values for Σ_t in each bloc have a significant impact on the radiation intensity. Also, the different zenith angles of the incoming radiation can clearly be seen.

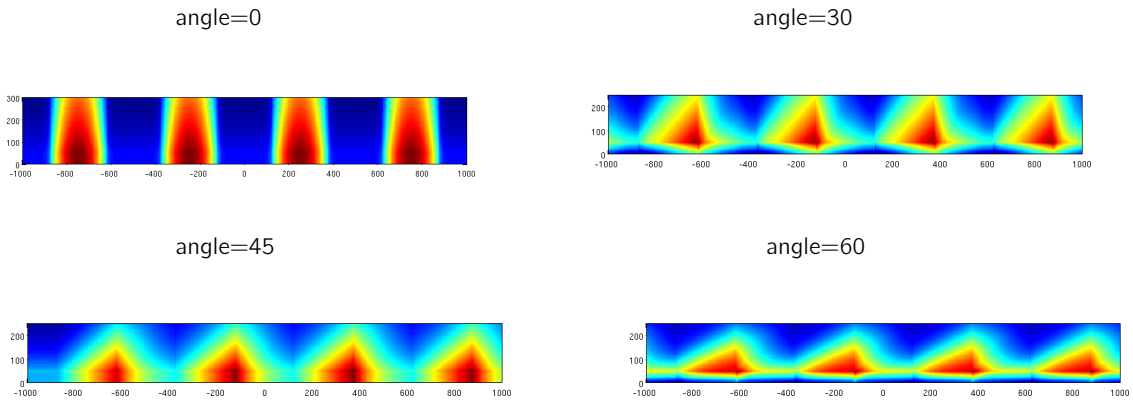

Figure 5. $\varepsilon = 0.03$ with different angles.

6.2.2. MMCR-Cloud In this section, we perform a simulation using an optical depth field which is given by experimental data available from the I3RC project. Figure 6 shows the obtained values of the optical depth $\sigma(x)$ which we choose for $\Sigma_t(x)$.

Now we perform two different simulations with a zenith angle of 0 and 60 degrees, $\varepsilon = 0.03$ and $\kappa = 0.85$. The angle is again simulated as in the previous case. Moreover, a source term $Q = 1$ everywhere on the domain describes incoming solar radiation. We see that the results given on figures 7 and 8 look similar to a real-world atmospheric cloud.

7. Conclusion and Outlook

In this paper we presented numerical schemes for the P1- and M1-moment model of a non-classical radiative transfer equation. Since an atmospheric cloud may have optically thick regions, we introduced a diffussive scaling and showed that the diffusion limits of the moment models and the original equations agree. The schemes were proven to be asymptotic preserving, admissible and realizable both for the explicit and the implicit discretization of the pseudo-time variable. The proposed source iteration-like method becomes slow in the optical thick case, but a suitable initialisation can help to overcome this problem. Numerical tests in the 1D and 2D case show good agreement with the exact solution and show that simulations yield realistic results.
Future work with this model will be on:

- Acceleration of the iterative method. The method of diffusion synthetic acceleration (DSA,[7]) may be fitted to this problem in the 1D case.
- Extension of the model to the case of inhomogeneous background media and frequency or energy dependence of the angular flux. This will enable us to work with further, more complex I3RC test-cases [21].
- Once a faster forward solver is available, a parameter identification for $\Sigma_t(s)$ or $p(s)$ will be done using methods from the theory of PDE-constrained optimization and measured data for the photon path-length in atmospheric clouds (see e.g. [5]).

References

1. A.B. Kostinski, *On the Extinction of Radiation by a Homogeneous but Spatially Correlated Random Medium*, J. Optical Society of America, A. 18, no.8, 1929–1933, (2001).
2. E. W. Larsen, *A generalized Boltzmann equation for "non-classical" particle transport*, Joint Int. Meeting on Math. Comp. & Supercomp. in Nucl. App., Monterey, California, on CD-ROM, Am. Nuc. Soc., LaGrange Park, IL (2007).
3. E. W. Larsen, R. Vasques, *A generalized linear Boltzmann equation for non-classical particle transport*, Vol. 112 (4), pp. 619 - 631 (2011). DOI: http://dx.doi.org/10.1016/j.jqsrt.2010.07.003
4. M. Frank, T. Goudon, *On a generalized Boltzmann equation for non-classical particle transport*, Kinet. Relat. Models 3, 395–407 (2010).
5. O. Funk, K. Pfeilsticker, *Photon path length distributions for cloudy skies - oxygen A-Band measurements and model calculations*, Ann. Geophys. 21, 615-626 (2003).
6. E. W. Larsen, J. E. Morel, W. F. Miller, Jr., *Asymptotic Solutions of Numerical Transport Problems in Optically Thick, Diffusive Regimes*, J. of Comp. Phys. 69, 283–324 (1987).
7. M. L. Adams, E. W. Larsen, *Fast iterative methods for discrete-ordinates particle transport calculations*, Progr. in Nucl. En. 40, No. 1, 3–159 (2002).
8. S. Jin, *Efficient Asymptotic-Preserving (AP) Schemes For Some Multiscale Kinetic Equations*, SIAM J. Sci. Comp 21, 441–454 (1999).
9. S. Chandrasekhar, *On the radiative equilibrium of a stellar atmosphere*. II. Astrophys. J. 100, 76-86 (1943).
10. E. T. Jaynes, *Information Theory and Statistical Mechanics*, Phys. Rev. 106, 620-630 (1957).
11. G. N. Minerbo, *Maximum entropy Eddington factors*, J. Quant. Spectrosc. Radiat. Transf. 20, 541-545 (1978).
12. B. Dubroca, J.-L. Feugeas, *Étude théorique et numérique d'une hiérarchie de modèles aux moments pour le transfert radiatif*, C. R. Acad. Paris, 915-920 (1999).
13. C. D. Levermore, *Moment closure hierarchies for kinetic theories*, J. Statist. Phys. 83, no. 5-6, 1021-1065 (1996).
14. E. W. Larsen, J. E. Morel, J. M. McGhee, *Asymptotic Derivation of the Multigroup P_1 and Simplified P_N Equations with Anisotropic Scattering*, Nucl. Sci. Eng. 123, 328–342 (1996).
15. A. Harten, P. Lax, B. van Leer, *On upstream differencing and Godunov-type schemes for hyperbolic conservation laws*, SIAM Review, Vol. 25, No. 1, 35 – 61 (1983).
16. F. Golse, S. Jin, C. D. Levermore, *The convergence of numerical transfer schemes in diffusive regimes I: The discreteordinate method*, SIAM J. Numer. Anal. 36, pp. 1333-1369 (1999).
17. C. Buet, S. Cordier, *An asymptotic preserving scheme for hydrodynamics radiative transfer models*, Numerische Mathematik, Vol.108, No. 2 , pp. 199–221 (2007). DOI: 10.1007/s00211-007-0094-x
18. C. Berthon, P. Charrier, B. Dubroca, *An HLLC scheme to solve the M1 model of radiative transfer in two space dimensions*, J. Sci. Comput., 31. no. 3, pp. 347-389 (2007).
19. L. Gosse, G. Toscani, *Asymptotic-preserving & well-balanced schemes for radiative transfer and the Rosseland approximation* J. Num. Math., Vol. 98, 2, pp. 223 – 250 (2004).
20. D. Aregba-Driollet, M. Briani, R. Natalini *Time Asymptotic high order Schemes for dissipative BGK hyperbolic Systems*, arxiv:1207.6279v1 (2012).
21. R. F. Cahalan et al., *The I3RC - Bringing Together the Most Advanced Radiative Transfer Tools for Cloudy Atmospheres*, Bulletin of the American Meteorological Society 86, Issue 9, 1275–1293 (2005).

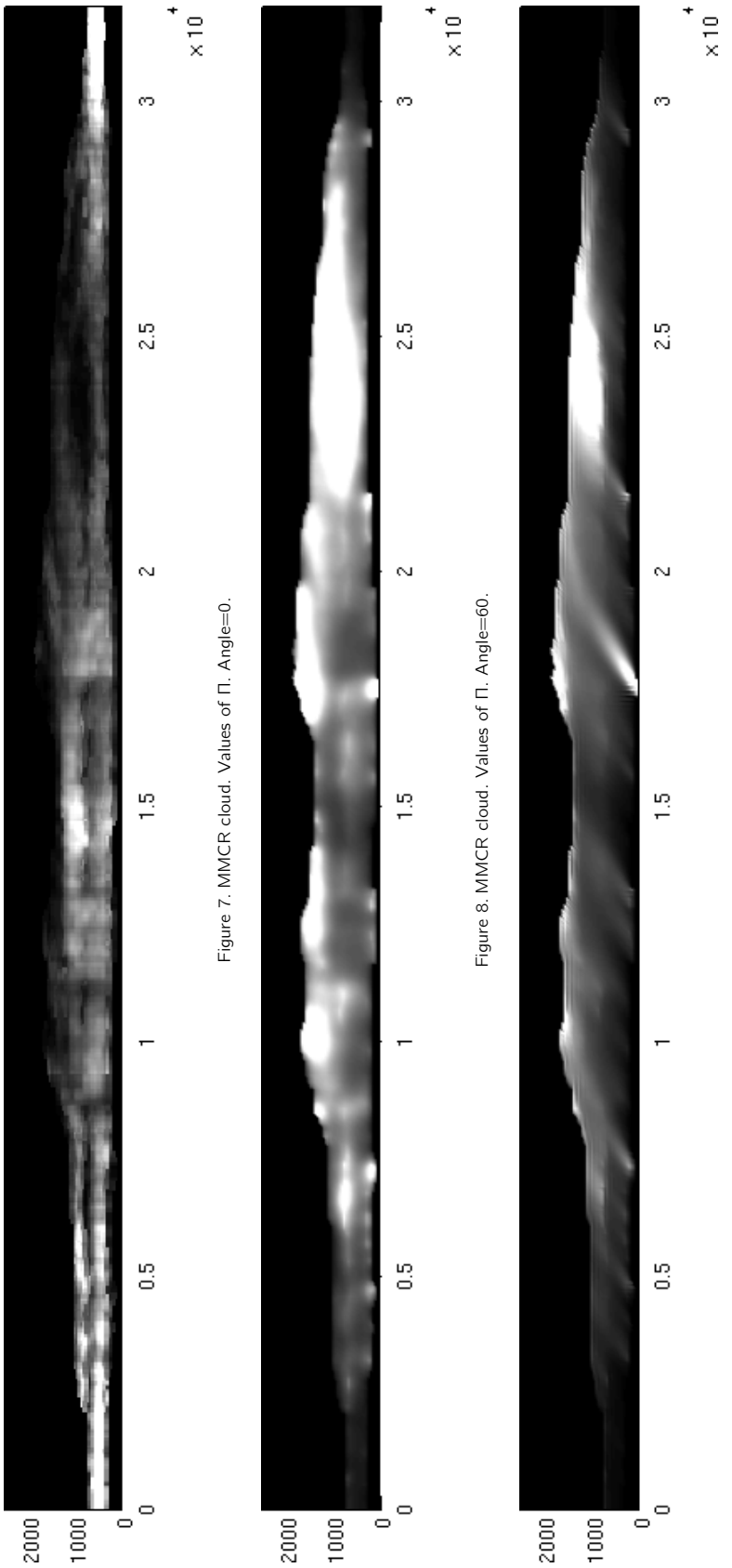

Figure 6. MMCR cloud. Values of $\Sigma_t(x)$.

Figure 7. MMCR cloud. Values of Π. Angle=0.

Figure 8. MMCR cloud. Values of Π. Angle=60.

